

# A DNA Fishhook Electrochemical Sensor Based on a Potassium Ferricyanide-Mediated Dual-Signal-Correlation Enhanced Electrocatalysis Reaction for a Simultaneous and Correlation Assay of Multiple Biomarkers

Guanyu Chen,<sup>¶</sup> Lilan Xu,<sup>¶</sup> Zhuhua Chen, Lifang Lin, Wenlu Wang, Mingzhu Chen, Weiming Sun, Xiaobing Huang,\* Xi Zhang,\* and Jinghua Chen\*



Cite This: <https://doi.org/10.1021/acssensors.4c03142>



Read Online

ACCESS |



Metrics & More



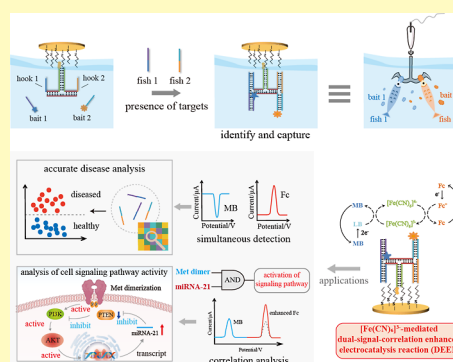
Article Recommendations



Supporting Information

**ABSTRACT:** Simultaneous detection and correlation analysis of multiple biomarkers in a single run are crucial to improving the detection specificity and indicate disease progression, but they remain a challenge. Herein, we propose a DNA fishhook electrochemical sensor based on the potassium ferricyanide-mediated dual-signal correlation enhanced electrocatalysis reaction (DEER). The designed T-shaped DNA fishhook scaffold has two “hooks” to recruit their respective “fish” (targets) with the help of the “fishing bait” (signal probes, Sp), resulting in the different targets and Sp being specifically captured by the DNA fishhook to the electrode interface, respectively. The proposed DEER not only effectively improves the detection sensitivity without introducing nucleic acid amplification but also can reflect the logical correlation between the targets. As proof of principle, the DNA fishhook sensor was successfully applied in the simultaneous detection of two related gene sequences of SARS-CoV-2 and the active-state assay of the PI3K/AKT signaling pathway. In general, our DNA fishhook sensor provides a meaningful potential tool for the sensitive simultaneous detection and correlation analysis of multiple targets.

**KEYWORDS:** DNA fishhook, electrochemical biosensor, simultaneous detection, correlation assay, multiple biomarkers, signaling pathway



Biomarkers are signposts of disease.<sup>1</sup> As the measurable indicators, a myriad of biomarkers depict the presence, severity, and intensity of disease.<sup>2</sup> With enormous developments in molecular medicine, detection of biomarkers has shown great prospects in early diagnosis, predicting disease, or prognostic evaluation. Especially, multiple biomarker assays that simultaneously detect multiple targets in a single run rapidly offer more information at a lower cost and smaller sample size to further identify the subtypes of diseases, virus variants, etc., or to reduce false-positive rates and improve diagnostic accuracy.<sup>3,4</sup> In addition, biomarkers, as the key signaling molecules, can regulate the intracellular signaling transduction pathways and reflect biological responses in cells.<sup>5</sup> The “crosstalk” among highly interconnected pathways allows them to come together to form a complex signaling network. Mapping the dynamic influence connections among biomarkers in the signaling network aids in a better understanding of the underlying molecular mechanisms and the development of therapeutics for diseases involving aberrant pathways, such as cancer and autoimmune diseases.<sup>6</sup>

In this context, numerous biosensors for the simultaneous detection of multiple biomarkers have been developed.<sup>7–9</sup> Among them, DNA electrochemical biosensors, as a cost-

effective, highly sensitive, universal, and user-friendly sensing platform, provide a powerful approach for the sensitive detection of multiple biomarker targets.<sup>10,11</sup> For DNA electrochemical biosensors, the key to realizing multitarget electrochemical detection lies in converting the abundance of different targets into a quantifiable current response in a single-electrode system.<sup>12</sup> The conventional method is to modify different single-stranded capture probes at the electrode interface to introduce corresponding electroactive molecules in the presence of specific targets and to generate signal responses at different potentials to distinguish the corresponding targets.<sup>13</sup> Yet, due to the interaction between DNA–DNA helices and the DNA base-gold surface, different flexible single-stranded DNA probes may be entangled with each other on the electrode interface<sup>14</sup> or lie flat on the gold surface instead

**Received:** November 7, 2024

**Revised:** April 1, 2025

**Accepted:** May 9, 2025

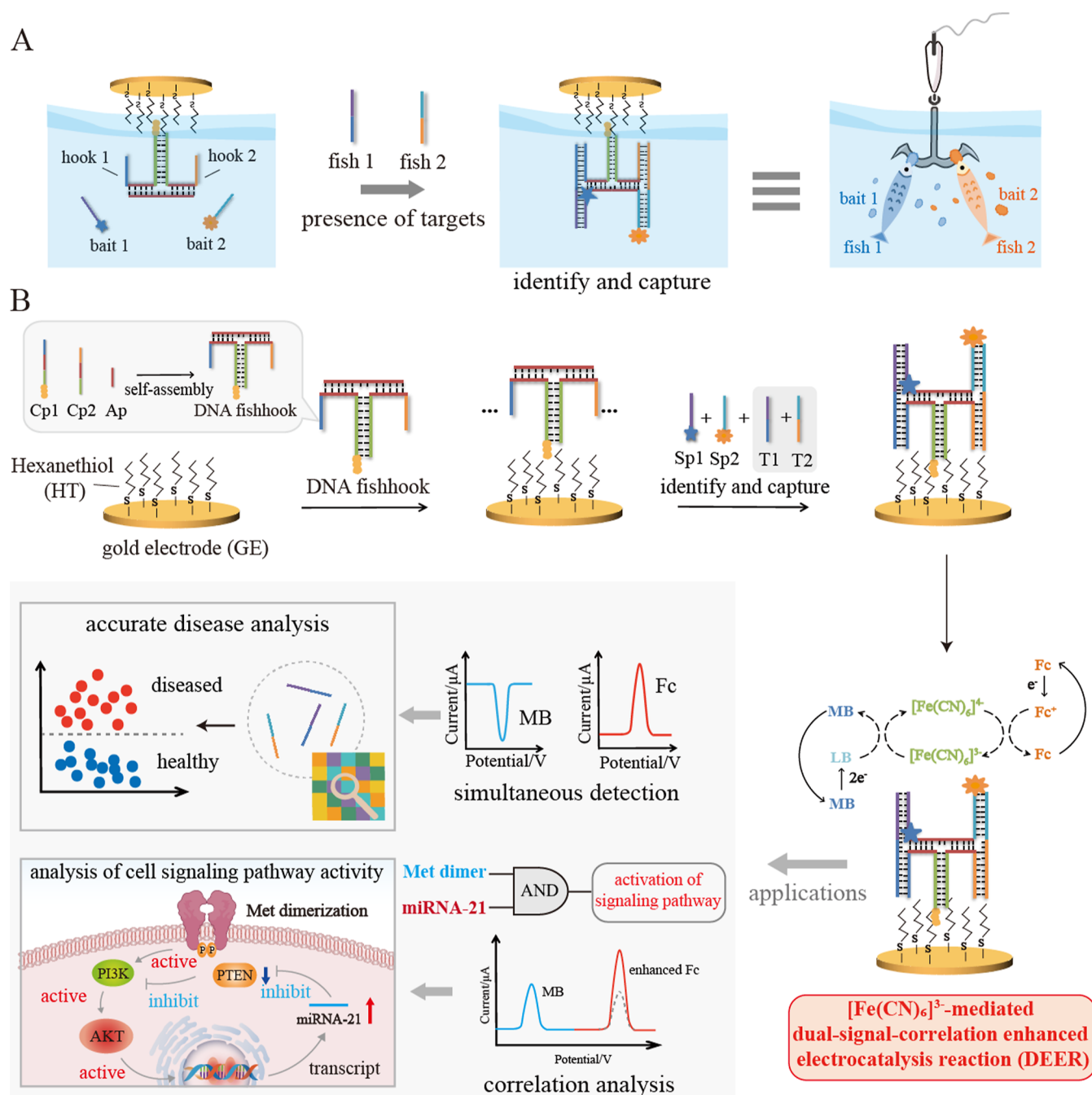


**Figure 1.** (A) Concept diagram of “fishing” multiple targets by the DNA fishhook biosensor. (B) Principles and applications for the multiple detection of targets based on a fishhook electrochemical biosensor.

of standing upright as required,<sup>15</sup> resulting in low accessibility and capture efficiency of the target. Moreover, it is difficult for different DNA capture probes to assemble on the electrode surface in a specific ratio, which may result in a very high density of one probe and a very low density of the other. This uncontrollable distribution of different probes will lead to high measurement errors and nonrepeatability.<sup>14</sup>

In addition, to further improve sensing performance, these methods are often combined with DNA cyclic amplification techniques to realize ultrasensitive detection of targets.<sup>16,17</sup> However, for multitarget detection, each target needs to be amplified individually, which requires not only complex sequence design but also the avoidance of crosstalk between sequences.<sup>18,19</sup> Although studies have been conducted to

improve the sensitivity by introducing nanoparticles to increase the specific surface area of the electrode for sensitive detection without nucleic acid amplification,<sup>9,20–22</sup> the preparation process of nanoparticles is complex and expensive, which further affects the convenience and cost of analysis. Furthermore, these methods are designed for quantifying independent targets but are not suitable for correlation analysis among multiple targets. Some methods employing DNA logic gates can do correlation analysis but not simultaneous quantification of independent targets.<sup>23,24</sup> Therefore, it is urgent to develop an electrochemical sensor that enables simple, rapid, accurate, cost-effective, and nucleic acid-amplification-free multiple target detection and correlation analysis.

To deal with the above-mentioned issues, we designed a DNA “fishhook” for simultaneous multiple target electrochemical detection in this work. The T-shaped DNA fishhook scaffold has well-controlled spatial orientation and nanoscale distance control ability to regulate the homogeneity of different capture probes at the electrode interface, thereby avoiding mutual entanglement.<sup>25,26</sup> In order to “fish” multiple targets, as shown in Figure 1A, the overhanging sequences on either side of the T-shaped DNA scaffold are used as two “hooks” to capture different targets. When the targets exist, the “bait” sequences (signal probe) specifically bind to their respective “fish” (target) through base complementary pairing and induce it to be captured by the DNA fishhooks at the electrode interface, resulting in further enrichment of MB and Fc at the electrode interface. Since two different “hooks” are integrated in one DNA nanostructure in a 1:1 ratio, the uniformity of probe distribution on the electrode is greatly improved, which is beneficial to the detection accuracy. And, the two “hooks” do not interfere with each other, allowing independent detection of two different targets. Moreover, the modular design of the DNA fishhook makes it universal, which can be used for the detection of other targets by simply modifying the “hook” sequence.

Considering that DNA nanostructures may hinder the electron transfer between the electrode and the electroactive molecule by increasing the resistance of the electrode to reduce the detection sensitivity, we proposed a  $[\text{Fe}(\text{CN})_6]^{3-}$ -mediated dual-signal-correlation enhanced electrocatalysis reaction (DEER). The DEER achieves simultaneous signal amplification of MB and Fc and further enhances reaction efficiency by rational use of the reaction products. In addition, the enhanced signal is due to the concurrence of MB and Fc, and it can be designed to conform to the logical relationships in “AND” logic gates. These features enable the DEER to be used for the simultaneous detection of multiple targets and correlation analysis between targets. Interestingly, in the DEER, the inhibition of electron transfer by DNA fishhook does not reduce the detection sensitivity, instead, it can cooperate with the hydrophobic hexanethiol (HT) self-assembly layer to passivate the electrode to avoid the interference of electron transfer between  $[\text{Fe}(\text{CN})_6]^{3-}$  and the electrode interface.<sup>27</sup> Therefore, only a simple incubation step is required to produce a significant current response.

As a proof of concept, the DNA fishhook biosensor was successfully applied to the simultaneous detection of the SARS-CoV-2 RDRP gene and N gene fragment and the correlation analysis of the miRNA-21 between Met dimer in the PI3K/AKT signaling pathway. Overall, this work developed a simple, rapid, sensitive, amplification-free strategy for multitarget detection and correlation analysis, which is promising in a broader application of the biomarker assay.

## EXPERIMENT SECTION

**Self-Assembly of the DNA Fishhook.** After centrifugation (6000 rpm/min), the DNA oligonucleotides were dissolved in TE buffer and diluted in  $1 \times \text{TAE}/\text{Mg}^{2+}$  buffer (containing 10 mM Tris, 1 mM EDTA-2Na, 50 mM NaCl, and 12.5 mM  $(\text{CH}_3\text{COO})_2\text{Mg}$ ). For preparation of the DNA fishhook, 5  $\mu\text{M}$  capture probes (Cp1, Cp2) and auxiliary probe (Ap) were well mixed in  $1 \times \text{TAE}/\text{Mg}^{2+}$  buffer together and annealed in a metal bath. The annealing method is as follows: The DNA fishhook was incubated for 5 min at 95 °C. Then

the temperature was decreased at 1 degree per minute until reaching 25 °C and subsequently cooled to 4 °C for 1 h.

**Pretreatment of the Electrode and Preparation of the Sensor.** The surface of the gold electrode was polished with 0.3 and 0.05  $\mu\text{m}$  alumina. The electrode was then immersed in ultrapure water and ethanol, respectively, and ultrasonically cleaned for 3 min. After drying with nitrogen, the electrode was immersed in 0.5 M  $\text{H}_2\text{SO}_4$  to obtain a cyclic voltammetry (CV) curve by an electrochemical workstation (CHI 660E, Shanghai Chenhua Instrument Co., Ltd.) until the curve was stable. Afterward, the pretreated gold electrode was immersed in the 5 mM HT and incubated at room temperature for 1 h to cover a tight HT assembly layer on the electrode surface. Four  $\mu\text{L}$  of the above-mentioned DNA fishhook was added dropwise onto the dry electrode surface for 1 h at room temperature. The DNA fishhook assembled electrode was successfully fabricated.

**Electrochemical Assay of Multiple Targets.** For the assay of the multiple targets, 4  $\mu\text{M}$  Sp1 and 2  $\mu\text{M}$  Sp2 were mixed with nuclease-free water; T1 and T2 were diluted uniformly in  $1 \times \text{TAE}/\text{Mg}^{2+}$  buffer and then added dropwise onto the DNA fishhook assembled electrode reaction for 30 min at room temperature. After reaction, the electrode was immersed in PBS buffer (containing 10 mM  $[\text{Fe}(\text{CN})_6]^{3-}$ ) for the electrochemical assay. CV and square wave voltammetry (SWV) were used for electrochemical scanning with the following settings. CV: potential range of  $-0.5 \sim 0.7$  V, the standing time was 2 s, the scanning speed was 0.1 V/s, and the sampling interval was 1 mV. SWV: a potential range of  $-0.5 \sim 0.7$  V, a voltage increase of 0.004 V, an amplitude of 0.025 V, a frequency of 50 Hz, and a standing time of 2 s.

## RESULTS AND DISCUSSION

**The Principle of DNA Fishhook for Multitarget Detection and Correlation Analysis.** As shown in Figure 1B, the DNA fishhook is formed by the self-assembly of Cp1, Cp2, and Ap. The prehybridized DNA fishhook was immobilized on the HT assembly electrode through the hydrophobic interaction between the terminally modified cholesterol and HT. In the absence of “fish” targets, the “fishing baits”, MB-labeled signal probe 1 (Sp1) and Fc-labeled signal probe 2 (Sp2), are not captured by the DNA fishhook. In contrast, when only one “fish”, the target 1 (T1), is present, Sp1 binds to its specific sequence domain to form T1-Sp1, which is then specifically captured by one of the hooks (Cp1) at the electrode interface. Under the electrocatalysis reaction, a significant catalytic current of MB is produced. Due to the absence of another “fish”, target 2 (T2), Sp2 cannot be directly hybridized to Cp2 and therefore does not produce an Fc signal. Similarly, in the presence of T2 but not T1, only Fc-labeled Sp2 is captured onto the electrode interface, thus generating only the catalytic current of Fc. When two types of “fish” (T1 and T2) coexist, both Sp1 and Sp2 are captured at the electrode interface, resulting in the generation of both MB and Fc catalytic currents. Notably, the coexistence of MB and Fc will trigger the DEER, further enhancing the reduction peak of MB and the oxidation peak of Fc. Based on the change of catalytic current, the simultaneous detection of T1 and T2 can be realized, which can be used to improve the accuracy of disease diagnosis. The enhanced signal caused by the coexistence of MB and Fc also conforms to the AND logic relationship, which can be used to analyze the logical correlation of multiple targets. The logical correlation analysis

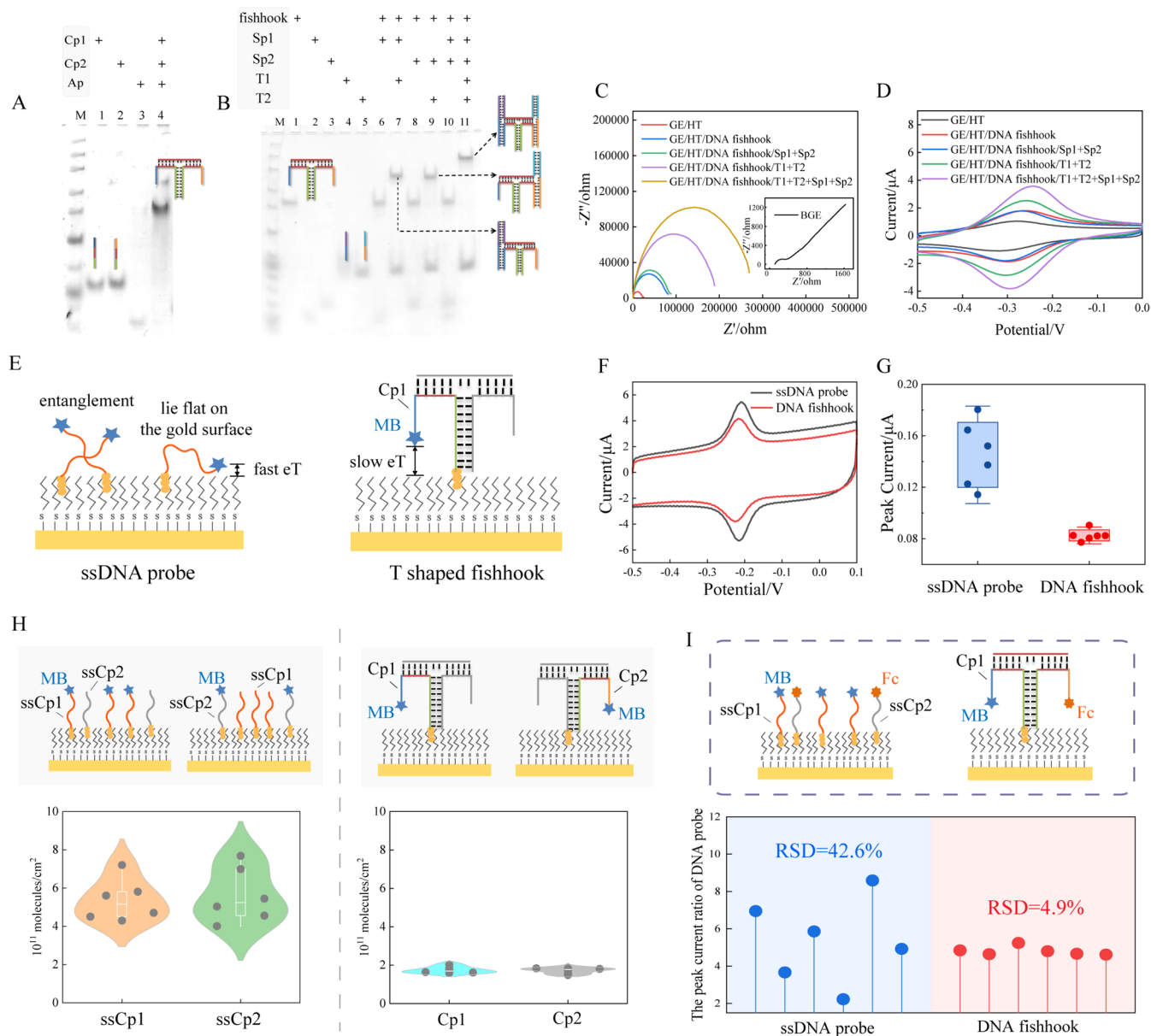


**Figure 2.** PAGE characterization of (A) the DNA fishhook and (B) the feasibility of the fishhook for dual target detection. (C) EIS and (D) CV characterization of the DNA fishhook-based biosensor. (E) Schematic illustration of the electrode interface of ssDNA probes or the DNA fishhook. The (F) CV characterization and the (G) peak current of ssDNA probes and DNA fishhook at the electrode interface. (H) The calculation of assembly density of different DNA probes at the electrode interface. (I) Characterization of the ratio of different probes assembled on the electrode interface.

of key molecules in the cell signaling pathway can be further used to feed back the active state of the cell signaling pathway and realize the dynamic monitoring of disease progression.

**The Characterization of the DNA Fishhook.** The rationality of the design of the DNA fishhook and the target capture function of the fishhook were characterized by NUPACK fitting (Figures S1 and S2) and PAGE.<sup>28</sup> The results of PAGE in Figure 2A showed that, after annealing, the mixture of Cp1, Cp2, and Ap produced a large molecular weight band, indicating the successful preparation of the DNA fishhook scaffold. Figure 2B shows that Sp1 cannot directly hybridize with the fishhook (lane 6). Only when T1 was present, T1, Sp1, and fishhook hybridized to form T1–Sp1–fishhook, resulting in a new band with larger molecular weights observed in lane 7. Likewise, Sp2 cannot hybridize with

fishhook (lane 8). Only when T2, Sp2, and fishhook structures are mixed can new bands be generated (lane 9). In lane 10, the mixture of Sp1, Sp2, and fishhook did not produce new bands, indicating that the fishhook could not hybridize with Sp1 and Sp2 in the absence of T1 and T2. In lane 11, a new band was clearly observed with a molecular weight greater than that of the bands in lane 7 and lane 9, indicating that the addition of T1 and T2 led to the hybridization of Sp1 and Sp2 with the fishhook. The PAGE results suggested that the designed strategy for multitarget detection is feasible.

Electrochemical impedance spectroscopy (EIS) was performed to characterize the assembly of the DNA fishhook at the electrode interface and its feasibility for dual-target detection. As shown in Figure 2C, the bare gold electrode (BGE) had good conductivity, resulting in an exceedingly low

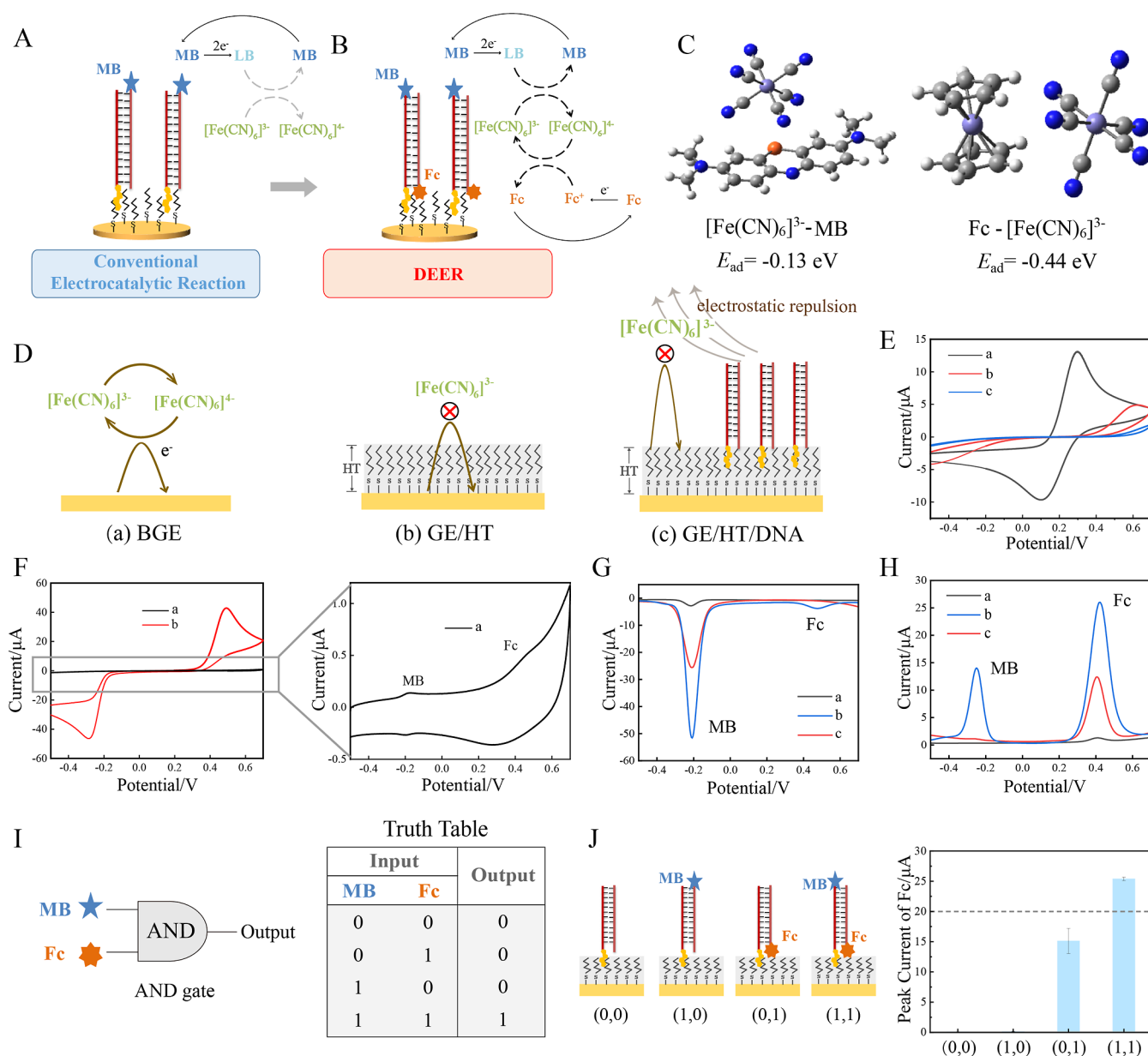


**Figure 3.** Feasibility analysis of the DEER. (A) Mechanism of the conventional  $[\text{Fe}(\text{CN})_6]^{3-}$ -mediated MB electrocatalytic reaction and (B) DEER. (C)  $E_{\text{ad}}$  values of  $[\text{Fe}(\text{CN})_6]^{3-}$ -MB and  $\text{Fc}-[\text{Fe}(\text{CN})_6]^{3-}$  complexes. (D) The schematic diagram and (E) CV characterization of HT and DNA synergistically blocking the electron transfer between  $[\text{Fe}(\text{CN})_6]^{3-}$  and the electrode: (a) BGE; (b) GE/HT; (c) GE/HT/DNA; (F) CV characterization of the DEER for simultaneously signal amplification of MB and Fc: (a) without  $[\text{Fe}(\text{CN})_6]^{3-}$ ; (b) with  $[\text{Fe}(\text{CN})_6]^{3-}$ . SWV characterization of the DEER for (G) MB and (H) Fc: (a) without  $[\text{Fe}(\text{CN})_6]^{3-}$ ; (b) DEER; (c) conventional electrocatalytic reaction. The construction of the “AND” logic gate based on the DEER. (I) “AND” logic gate and the truth table. (J) Various input modes and their oxidation peak current.

charge transfer resistance ( $R_{\text{ct}}$ ). Due to the fact that HT can be tightly packed at the electrode interface and greatly hinder the electron transfer between  $[\text{Fe}(\text{CN})_6]^{3-/4-}$  and the electrode interface, the modification of HT resulted in an evident increase in  $R_{\text{ct}}$ . After incubating the DNA fishhook on the HT packed electrode, the  $R_{\text{ct}}$  further increased due to the repulsion of  $[\text{Fe}(\text{CN})_6]^{3-/4-}$  by the negatively charged DNA phosphate backbone, indicating the successful assembly of the fishhook at the electrode surface. In the absence of T1 and T2, the addition of Sp1 and Sp2 did not cause significant changes in  $R_{\text{ct}}$ , indicating that Sp would not be immobilized on the electrode in the absence of the target. In contrast, the addition of T1 and T2 to the electrode surface induced an increase in

$R_{\text{ct}}$ , indicating the targets could be captured at the electrode interface via the DNA fishhook. The subsequent addition of Sp1 and Sp2 to the electrode led to a further increase in  $R_{\text{ct}}$ , suggesting the immobilization of Sp1 and Sp2 at the electrode interface. These results confirm the successful assembly of a DNA fishhook at the electrode interface and its ability to detect double targets. In addition, we used RuHex as an electrochemical indicator of DNA for further characterization, which is also in agreement with this result (Figure 2D).

Compared with the ssDNA probe, the rigid stem-like structure of the DNA fishhook can keep it upright at the interface and control the spatial distance of the probe to reduce the probe lying flat or entanglement on the electrode surface

(Figure 2E). To verify this, we labeled MB at the end of ssDNA and DNA fishhook and compared their signal responses at the electrode interface. As per the CV result shown in Figure 2F, the ssDNA probe displayed a higher redox current response than the DNA fishhook. The corresponding peak current of the ssDNA probe was also higher than that of the DNA fishhook, and the current was more dispersed (Figure 2G). This may be because the flexible ssDNA tends to lie flat on the electrode surface, resulting in end-labeled MB and electrode surface attachment and direct electron transfer. This direct electron transfer is more rapid than electron tunneling or hopping through the DNA strand (such as the DNA fishhook), leading to a more pronounced signal response.<sup>29</sup> In addition, the more dispersed current of ssDNA probes may be due to the uneven assembly caused by the entanglement of flexible single DNA strands.<sup>14</sup> In contrast, the upright conformation of the T-shaped fishhook leads to a smaller and more constant current response.

For multiple target detection, different DNA capture probes are homogeneously assembled at the electrode interface in a specific ratio, which is important for improving the detection accuracy. To quantify the assembly homogeneity of different DNA probes, we calculated the assembly density of the two ssDNA probes (ssCp1, ssCp2) and two “hooks” (Cp1, Cp2) of the DNA fishhook at the electrode interface, respectively (the calculation method is shown in Figure S3). The calculation results in Figure 2H showed that even if ssCp1 and ssCp2 were mixed at the same concentration, their assembly density at the electrode surface still showed large dispersion in 6 parallel experiments. This dispersion may be due to the fact that the two probes cannot be assembled in a specific ratio at the electrode interface, resulting in a high density of one probe and a low density of the other. In contrast, the assembly densities of Cp1 and Cp2 are relatively concentrated, indicating that they have good homogeneity.

Subsequently, we further explore the assembly ratio of different probes at the electrode surface by recording the ratio of peak current of end-labeled MB and Fc. As shown in Figure 2I, when ssCp1 and ssCp2 were mixed at a 1:1 ratio, the actual assembled proportion of ssCp1 and ssCp2 at the electrode interface was not yet constant, and the RSD in different experimental batches was as high as 42.6%. The inhomogeneity of ssDNA probes on the electrode may result in high measurement error and irreproducibility. Compared with the ssDNA probe, the two probes of Cp1 and Cp2 are integrated into the DNA fishhook by hybridization, making the assembly ratio of the probe at the electrode interface constant. The relative standard deviation (RSD) of experimental results of 6 batches was only 4.9%. These results indicate that DNA fishhooks formed by different capture probes in a specific ratio have better assembly uniformity than the ssDNA probe.

**Design of the DEER.** Despite many advantages in multiple detection,<sup>9</sup> DNA nanostructures at the electrode interface may hinder electron transfer and reduce the signal response. Notably, the  $[\text{Fe}(\text{CN})_6]^{3-}$ -mediated electrocatalytic reaction provides a simple, effective chemical signal amplification manner for electrochemical detection, which can use the inhibition of  $[\text{Fe}(\text{CN})_6]^{3-}$  electron transfer by DNA nanostructures to improve the signal amplification efficiency. The conventional electrocatalytic signal amplification reaction is carried out between  $[\text{Fe}(\text{CN})_6]^{3-}$  and a single type of electroactive molecule.<sup>30</sup> For example, in the electrocatalytic reaction of  $[\text{Fe}(\text{CN})_6]^{3-}$  and MB (Figure 3A), MB is reduced

to leucomethylene blue (LB) driven by voltage, and LB reduces  $[\text{Fe}(\text{CN})_6]^{3-}$  to generate  $[\text{Fe}(\text{CN})_6]^{4-}$ , resulting in the regeneration of MB and allowing the electrocatalytically cyclic redox (MB-LB-MB) reaction to continue. Theoretically, this process can be repeated until all  $[\text{Fe}(\text{CN})_6]^{3-}$  in solution has been reduced to  $[\text{Fe}(\text{CN})_6]^{4-}$ .<sup>31</sup> However, a single type of electroactive molecule at one electrode interface cannot respond to the concentration changes of the two targets simultaneously. It is necessary to find two electroactive molecules that both can be amplified by the electrocatalytic reaction and have a relatively independent electrochemical response potential. Thus, we proposed the DEER to realize the amplification of two electroactive molecules by rationally utilizing the products of the electrocatalytic reaction ( $[\text{Fe}(\text{CN})_6]^{4-}$ ). As shown in Figure 3B, an additional electroactive molecular Fc was introduced into the electrocatalytic reaction of  $[\text{Fe}(\text{CN})_6]^{3-}$  and MB. We hypothesized that  $\text{Fc}^+$  can be reduced by  $[\text{Fe}(\text{CN})_6]^{4-}$ , which led to the regeneration of Fc and  $[\text{Fe}(\text{CN})_6]^{3-}$  and facilitated the redox of  $\text{Fc}-\text{Fc}^+$ . The regenerated  $[\text{Fe}(\text{CN})_6]^{3-}$  can recatalyze the redox reaction of MB-LB. As a result, the cascade recycling of  $[\text{Fe}(\text{CN})_6]^{3-}$  not only allows the simultaneous electrocatalytic reaction of Fc and MB but also helps to further increase their electrocatalytic signals.

**Theoretical Calculation of the DEER.** In order to test our hypothesis, the feasibility of the electrocatalytic reaction between MB, Fc, and  $[\text{Fe}(\text{CN})_6]^{3-}$  was investigated by theoretical calculations. Since the electron transfer between MB, Fc, and  $[\text{Fe}(\text{CN})_6]^{3-}$  is the core of the electrocatalytic reaction, it usually occurs between substances that can bind to each other.<sup>32</sup> The adsorption energy ( $E_{\text{ad}}$ ) between  $[\text{Fe}(\text{CN})_6]^{3-}$ , MB, and Fc was calculated by density functional theory (DFT), to verify whether they are capable of transfer by mutual binding (the more negative the  $E_{\text{ad}}$  value, the higher the binding capacity between substances). As shown in Figures S4 and 3C, the most stable geometric structures of MB, Fc, and  $[\text{Fe}(\text{CN})_6]^{3-}$  monomers and  $[\text{Fe}(\text{CN})_6]^{3-}$ -MB and  $[\text{Fe}(\text{CN})_6]^{3-}$ -Fc complexes were obtained by optimization. The calculated  $E_{\text{ad}}$  values of  $[\text{Fe}(\text{CN})_6]^{3-}$ -MB and  $[\text{Fe}(\text{CN})_6]^{3-}$ -Fc complex were  $-0.13$  eV and  $-0.44$  eV, respectively (Figure 3C). The  $E_{\text{ad}}$  values of both complexes were negative, indicating that they can bind to each other.<sup>33,34</sup>

The theoretical feasibility of the DEER was further confirmed by calculating the vertical ionization energy (VIE) of LB,  $[\text{Fe}(\text{CN})_6]^{3-}$ ,  $\text{Fc}^+$ , and  $[\text{Fe}(\text{CN})_6]^{4-}$ . The smaller the VIE of a compound, the stronger the reducibility it has. As shown in Table S1, the VIE of LB (4.68 eV) is less than the VIE of  $[\text{Fe}(\text{CN})_6]^{3-}$  (7.49 eV), indicating that  $[\text{Fe}(\text{CN})_6]^{3-}$  can be reduced to  $[\text{Fe}(\text{CN})_6]^{4-}$  by LB. Similarly, the VIE of  $[\text{Fe}(\text{CN})_6]^{4-}$  (3.64 eV) is less than that of  $\text{Fc}^+$  (8.82 eV), indicating that  $\text{Fc}^+$  can be reduced to Fc by  $[\text{Fe}(\text{CN})_6]^{4-}$ . Although the VIE of LB is also smaller than that of Fc, it is hard for them to transfer electrons to each other. This is because MB and Fc are labeled at different ends of Sps and separated by a certain distance through the T-shaped fishhook, making it difficult for them to combine with each other. Additionally, the concentration of  $[\text{Fe}(\text{CN})_6]^{3-}$  in the solution is much higher than that of MB and Fc labeled at the electrode interface, so the LB generated by MB tends to react with  $[\text{Fe}(\text{CN})_6]^{3-}$ , rather than generate  $\text{Fc}^+$ . These results confirm the theoretical feasibility of the DEER.

**Feasibility of the DEER.** For validating the practical feasibility of the DEER, we constructed an MB and Fc

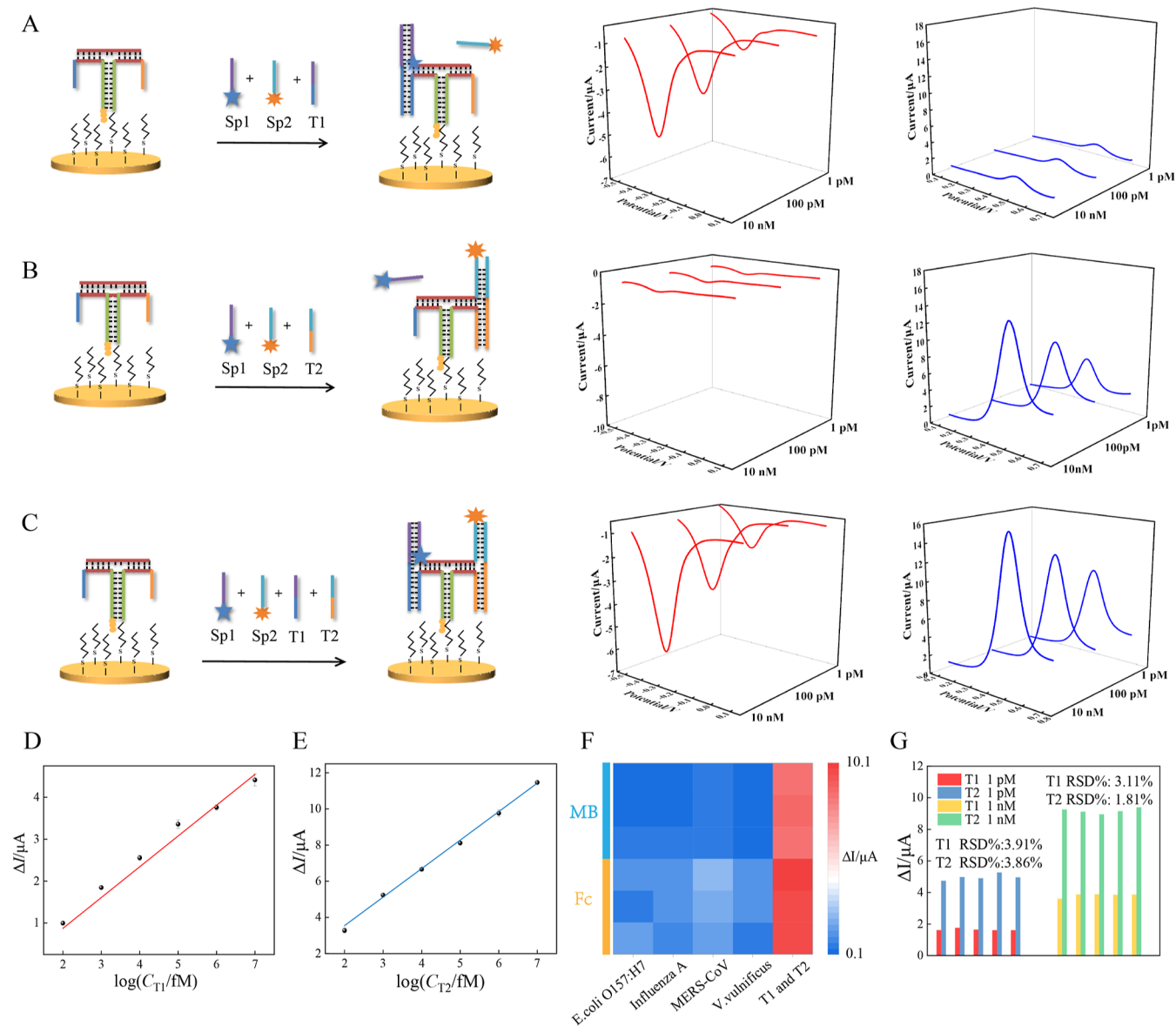


**Figure 4.** Feasibility of the fishhook sensor for simultaneous target detection. SWV characterization of the fishhook for detection of (A) T1, (B) T2, and (C) T1 and T2 coexistence. Standard curve of  $\Delta I$  at different logarithmic concentrations of (D) T1 and (E) T2. The (F) specificity and (G) reproducibility of the fishhook sensor.

modified double-stranded DNA model. As shown in Figure S5, cholesterol and MB-labeled Probe 1 (P1) were prehybridized with Fc-labeled Probe 2 (P2) to form a P1–P2 duplex and then immobilized at the electrode surface by the hydrophobic interaction between cholesterol and HT. To realize the DEER, it is necessary to prevent the interference of the fast electron transfer between  $[\text{Fe}(\text{CN})_6]^{3-}$  and the electrode (Figure S6). Our previous work has confirmed that hydrophobic HT can form a tightly packed self-assembled monolayer on the electrode surface, which can cooperate with negatively charged phosphate backbone of DNA, to isolate  $[\text{Fe}(\text{CN})_6]^{3-}$  to the periphery of the electrode by hydrophobic interaction and electrostatic repulsion, achieving efficient electrocatalytic signal amplification (Figure 3D).<sup>27</sup> Therefore, we first investigated and characterized the synergistic blocking effect of DNA and HT self-assembled monolayers on the electron transfer between  $[\text{Fe}(\text{CN})_6]^{3-}$  and the electrode. As shown in Figure 3E,  $[\text{Fe}(\text{CN})_6]^{3-}$  showed a symmetrical redox peak on the

BGE (curve a), indicating fast electron transfer between  $[\text{Fe}(\text{CN})_6]^{3-}$  and the electrode. After assembly of HT, the redox peak of  $[\text{Fe}(\text{CN})_6]^{3-}$  significantly decreased (curve b). With the further assembly of DNA, the redox peak of  $[\text{Fe}(\text{CN})_6]^{3-}$  disappeared completely (curve c), indicating that the electron transfer between  $[\text{Fe}(\text{CN})_6]^{3-}$  and the electrode has been effectively blocked by DNA and the HT self-assembled monolayer.

The feasibility of the DEER on the HT-assembled electrode was then characterized by CV and SWV. As shown in Figure 3F, in the absence of  $[\text{Fe}(\text{CN})_6]^{3-}$ , minor redox currents were observed at  $-0.25$  and  $0.4$  V in CV, resulting from the redox reaction of MB and Fc, respectively (curve a). However, significant reduction and oxidation peaks were observed in the presence of  $[\text{Fe}(\text{CN})_6]^{3-}$  at  $-0.25$  and  $0.4$  V, respectively, indicating that the DEER enhances the reduction current of MB and the oxidation current of Fc (curve b).

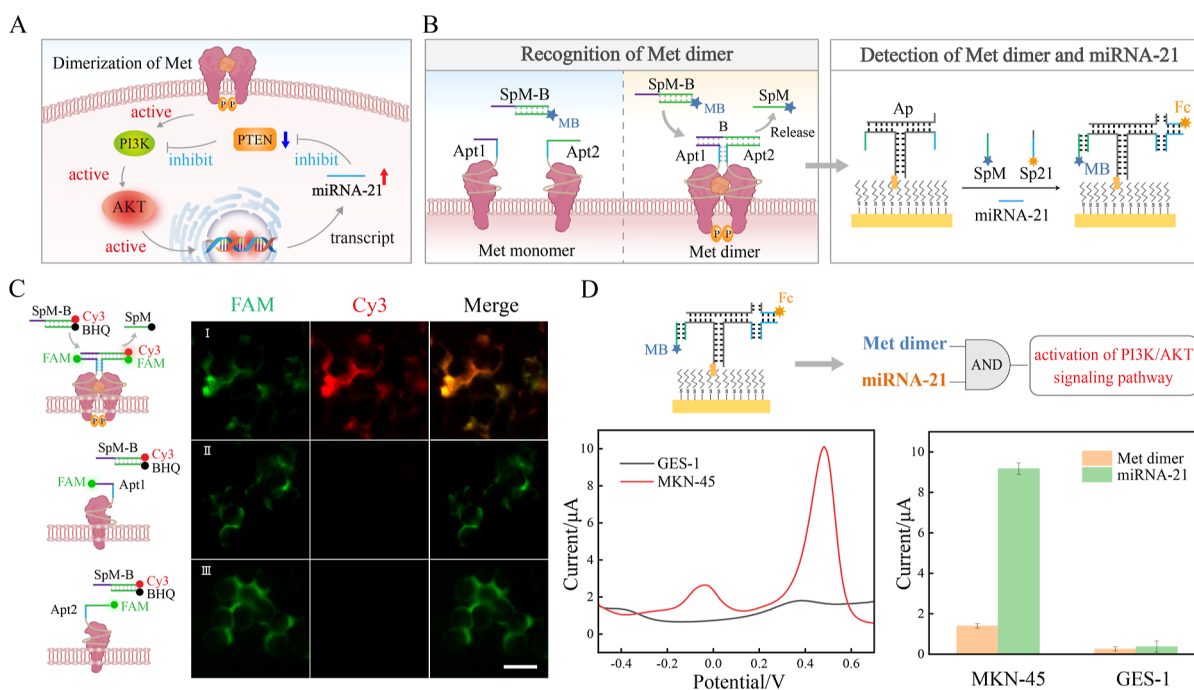


**Figure 5.** (A) Schematic diagram of the PI3K/AKT signaling pathway regulated by miRNA-21 and dimerization of Met. (B) The strategy based on a DNA fishhook electrochemical biosensor for the detection of the Met dimer and miRNA-21 logic correlation detection. (C) The feasibility characterization of the strategy for Met dimer recognition by fluorescence imaging system in the MKN-45 cells with different DNA probes: (I) Apt1, Apt2, and SpM-B; (II) Apt1 and SpM-B; (III) Apt2 and SpM-B. Scale bar = 4  $\mu\text{m}$ . (D) The correlation analysis of miRNA-21 and the Met dimer of MKN-45 and GES-1 cells by the DNA fishhook.

Considering that MB exhibits a more prominent reduction peak and Fc shows a more prominent oxidation peak, the reduction peak current of MB and the oxidation current peak of Fc were recorded by SWV to further evaluate the signal amplification ability of the DEER. As illustrated in Figure 3G,H, with the introduction of  $[\text{Fe}(\text{CN})_6]^{3-}$ , the reduction peak current of MB and oxidation peak current of Fc were increased significantly. The DEER increased the peak current of MB from 2.23  $\mu\text{A}$  (Figure 3G curve a) to 50.08  $\mu\text{A}$  (Figure 3G curve b) and increased the peak current of Fc from 0.56  $\mu\text{A}$  (Figure 3H curve a) to 24.82  $\mu\text{A}$  (Figure 3H curve b), which were a 22-fold and 44-fold increase, respectively. Moreover, as a result of recycling of  $[\text{Fe}(\text{CN})_6]^{3-}$ , the DEER displayed a higher signal amplification efficiency than conventional electrocatalytic reactions. The peak currents of MB (Figure 3G curve c) and Fc (Figure 3H curve c) in conventional electrocatalytic reaction were 24.40  $\mu\text{A}$  for MB and 11.14  $\mu\text{A}$  for Fc, which were only 48.72% and 44.88% of the DEER. The increase in current reflects the fact that the oxidized Fc molecules and reduced MB molecules have been recirculated in the electron-transfer reaction between Fc, MB, and  $[\text{Fe}(\text{CN})_6]^{3-}$ . These results suggest that the DEER can simultaneously improve the current signal response of MB and Fc.

Besides, the DEER can also reflect the logical correlation between MB and Fc molecules on the electrode, which provides a powerful tool for the correlation analysis of multiple targets. Specifically, when MB and Fc coexist, the DEER is triggered and the enhanced peak current is generated; this phenomenon is consistent with the “AND” logic correlation. Based on this, we construct an “AND” logic gate strategy to reflect the logical association between MB and Fc. As shown in Figure 3I, MB and Fc are used as logical inputs, which are

recorded as input “1” when they exist and as input “0” when they do not exist. The output signal is determined based on the oxidation peak current value of Fc ( $I_{\text{Fc}}$ ). As shown in Figure 3J, taking the current value of 20  $\mu\text{A}$  as the threshold, when  $I_{\text{Fc}}$  is greater than 20  $\mu\text{A}$ , the output is signal “1”; otherwise, the output is signal “0”. Since the enhanced  $I_{\text{Fc}}$  occurs only when MB and Fc are present together, the “1” output results are only achieved in the input modes of (1,1), which is consistent with the truth table of the “AND” logic gate. Therefore, the further signal amplification of the DEER caused by the simultaneous presence of MB and Fc can be used for the construction of an “AND” logic gate and correlation analysis of multiple targets.

**DNA Fishhook-Based Biosensor for the Detection of Multiple Targets.** To demonstrate that the DNA fishhook-based sensor can detect a single target independently or analyze two targets simultaneously, we applied the sensor for the detection of two SARS-CoV-2-related gene sequences (RDRP and N gene fragments, denoted as T1 and T2, respectively) at different concentrations. When T1 or T2 was present alone, as shown in Figure 4A,B, the peak current of MB or Fc gradually increased as the concentration of T1 or T2 increased, while the peak current of the other remained roughly unchanged. This is because only when T1 or T2 is captured by the DNA fishhook at the electrode interface can it bring MB-modified Sp1 or Fc-modified Sp2 to the electrode interface, thus increasing the current responses. These results indicated that the DNA fishhook-based sensor can be used for the independent detection of T1 or T2. Furthermore, as shown in Figure 4C, when both T1 and T2 were present, the electrochemical signals of MB and Fc gradually increased with the increase of T1 and T2 concentrations at the same time, which proved that the DNA fishhook-based sensor could also realize the simultaneous detection of T1 and T2.

To investigate the detection performance of the DNA fishhook-based biosensor, different concentrations of T1 and T2 were assayed under optimal conditions. (Optimization of the detection conditions is shown in Figure S7) With the increase of the T1 and T2 concentration, the peak current of MB and Fc gradually increased (Figure S8). In the concentration range of 100 fM–10 nM, signal response ( $\Delta I$ ) showed a good linear relationship with the logarithm of T1 and T2 concentrations, respectively (Figure 4D–E and Figure S9). The regression equations were  $\Delta I = 0.6747 (\log C_{T1}) - 0.2140$ ,  $r = 0.9944$ , and  $\Delta I = 1.599 (\log C_{T2}) + 0.2199$ ,  $r = 0.9993$ . According to the  $3\sigma$  rule, the calculated limit of detection (LOD) of the DNA fishhook-based sensor is 0.80 and 3.55 fM for T1 and T2, respectively. Compared to some recent multiple biomarker detection methods (Table S2),<sup>10,13,35–38</sup> our proposed DNA fishhook-based sensor has better sensitivity.

Furthermore, the specificity and reproducibility of the sensors were investigated. The specificity was evaluated by comparing the signal responses of various target sequences. As shown in Figure 4F, the  $\Delta I$  generated by T1 or T2 is at least 10-fold larger than that of other interference sequences, confirming good specific recognition ability for T1 and T2. Then, the reproducibility of the sensor was investigated by calculating the RSD of 5 repeated experiments. As shown in Figure 4G, the RSD for 1 pM T1 and T2 was 3.91% and 3.86%, respectively, and the RSD for 1 nM T1 and T2 was 3.11% and 1.81%, respectively, indicating the good reproducibility of the DNA fishhook-based sensor.

To validate the clinical applicability of the DNA fishhook-based sensor, T1 and T2 were dissolved in PBS-diluted saliva. The recovery rates were then calculated according to the linear relationship between  $\Delta I$  and  $\log C$ . As shown in Tables S3 and S4, the T1 recovery rates at concentrations of 100 fM, 10 pM, and 1 nM ranged from 96.35% to 105.10%, with respective RSD values of 4.13%, 2.92%, and 1.98%, respectively. The T2 recovery rates at the same concentrations ranged from 96.00% to 106.00%, with RSD values of 1.94%, 4.24%, and 4.97%, respectively.

**DNA Fishhook-Based Biosensor for Detection and Correlation Analysis of Cell Signaling Pathway-Related Molecules.** The cell signaling pathway is the molecular basis for the occurrence and development of diseases, which are regulated by a cascade of molecular reactions that bring out the functional attributes associated with the biological behaviors of cells.<sup>6,39,40</sup> For example, as shown in Figure 5A, the abnormal dimerization of Met on the cell surface can activate the PI3K/AKT signaling pathway, leading to the activation of transcription factor and the up-regulation of miRNA-21.<sup>41</sup> The abnormally up-regulated miRNA-21 can further activate the PI3K/AKT signaling pathway by downregulating the targeted PTEN, resulting in the proliferation of tumor cells.<sup>42</sup> Therefore, reflecting the pathway activity by the detection and correlation analysis of the abnormal changes of multiple key molecules (e.g., the Met dimer and miRNA-21) in the pathway is valuable to reveal the progression of diseases. To further demonstrate the feasibility of analyzing a logical relationship by our DNA fishhook, we took miRNA-21 and Met dimers as examples to study the activity of the PI3K/AKT signaling pathway.

The detection strategy is shown in Figure 5B. For the detection of the Met dimer, two Met aptamer probes (Apt1 and Apt2) were designed. They can induce mutual proximity

by binding to Met dimers, further triggering a strand displacement reaction to release the signal probe of Met dimers (SpM) from the SpM-B duplex. Subsequently, SpM was captured by the DNA fishhook on the electrode, producing an electrochemical signal to enable Met dimer detection. The detection of miRNA-21 is similar to the aforementioned strategy, where miRNA-21 can be captured by the DNA fishhook and recruit the Fc-labeled signal probe (Sp21) to the electrode. To improve the hybridization stability of Sp21 at the electrode interface, we here extended the 5 nt base sequence at the end of Ap. The resulting Fc signal is for miRNA-21 quantitative analysis. It is worth noting that, when miRNA-21 coexists with Met dimers, an enhanced oxidation signal of Fc will be generated due to the DEER. This correlation-enhanced response result helps reflect the logical relationship of the two targets in the pathway. Therefore, this strategy can not only quantify the expression levels of miRNA-21 and Met dimers independently but also analyze the activity of the cellular signaling pathway by reflecting the correlation between key signaling molecules.

The feasibility of the recognition of Met dimers and the release of SpM was characterized by the fluorescence imaging system. The gastric cancer cell MKN-45 (where the Met dimer is overexpressed) was selected as the study model. As shown in Figure 5C line I, after the incubation of FAM-labeled Apt1, Apt2, and SpM-B duplex, a bright FAM fluorescence was observed on the MKN-45 cell surface, indicating the successful binding of aptamers to Met. In addition, the fluorescence of Cy3 also emerged on the MKN-45 cell surface because the close proximity of Apt1 and Apt2 after binding to the Met dimer results in the hybridization of Cy3-labeled B with Apt1 and Apt2 as well as the release of BHQ-1-labeled SpM. In contrast, when only Apt1 (line II) or Apt2 (line III) was bound to the cell surface, no fluorescence of Cy3 was observed after the addition of SpM-B. This result further demonstrated the feasibility of the Met dimer recognition strategy. We also conducted a control experiment on normal gastric cell GES-1 with low Met expression. As shown in Figure S10, only faint green fluorescence of FAM and negligible fluorescence of Cy3 were observed on the surface of GES-1 cells, suggesting that the expression of Met receptor on the surface of the GES-1 cell membrane was low and Met mainly existed in the form of a monomer.

After using PAGE characterization to validate the feasibility of probe capture by a DNA fishhook (Figure S11), SWV was performed to further investigate the feasibility of the biosensor for the detection of the Met dimer and miRNA-21. To simplify the experiment, SpM was used as an indicator of the presence of Met dimers. As shown in Figure S12, compared with the blank, the presence of active SpM alone produced a significant MB oxidation peak, while the presence of miRNA-21 alone produced a significant Fc oxidation peak, indicating that the DNA fishhook biosensor could be used for independent quantification. In the coexistence of SpM and miRNA-21, MB and an enhanced Fc oxidation peak were produced, indicating that the DNA fishhook biosensor could also be used for the simultaneous detection and correlation analysis of the Met dimer and miRNA-21.

By the detection and correlation analysis of miRNA-21 and the Met dimer of cells, we further demonstrated that the DNA fishhook biosensor can be used to inform the activity status of the PI3K/AKT signaling pathway. As shown in Figure 5D, the MKN-45 cells displayed a large MB oxidation current and an

enhanced Fc oxidation current, suggesting that miRNA-21 and Met dimer were simultaneously highly expressed. In contrast, GES-1 cells displayed small MB and Fc oxidation currents, suggesting that their expression levels in GES-1 cells were low. This is because tumor cells can sustain the continuous activation of the PI3K/AKT signaling pathway by upregulating the expression of Met dimers and miRNA-21, leading to the dysregulation of programmed cell death protein expression and the abnormal proliferation of cells.

## CONCLUSION

In this paper, an electrochemical sensor based on DNA fishhook is proposed for the detection of multiple targets, offering the following advantages: (1) by employing two capture probes (Cp1 and Cp2) forming “fishhook” in a ratio of 1:1, the assembly uniformity of different capture probes at the electrode interface was effectively improved. (2) The DNA fishhook enables both independent detection of a single target and simultaneous detection of dual targets. (3) Compared with the traditional nucleic acid amplification detection, the DEER does not require complex pretreatment, expensive instruments, and materials, enabling straightforward and rapid simultaneous signal amplification of MB and Fc. The enhanced signal generated by the DEER can also be used for “AND” logic correlation detection. (4) The modular design of the DNA fishhook lends universality, allowing for the detection of any target simply by changing the sequence of the “hooks”. Future enhancements could involve the incorporation of some hydrophilic coatings (e.g., poly(ethylene glycol) (PEG) and zwitterionic polymers) to reduce the nonspecific electrode interface absorption and the modification of target recognition sites of Cp1 and Cp2 with the locked nucleic acid to further increase the target capture efficiency of the DNA fishhook-based biosensor. Overall, the proposed biosensor provides a superior and promising approach to biomarker detection and also provides a scalable strategy for the design of DNA electrochemical biosensors.

## ASSOCIATED CONTENT

### Supporting Information

The Supporting Information is available free of charge at <https://pubs.acs.org/doi/10.1021/acssensors.4c03142>.

Materials and reagents; cell culture; fluorescence imaging; NUPACK fitting of the DNA fishhook; calculation of DNA probe assembly density; calculation of adsorption energy; schematic diagram of the electrocatalytic reaction; schematic diagram of the model for verifying the DEER; optimization of detection conditions; SWV for T1 and T2 at different concentrations; feasibility characterization of the strategy for Met dimer recognition by fluorescence imaging system in the GES-1 cells; PAGE characterization of the capture feasibility for SpM and miRNA-21 by the DNA fishhook; SWV characterization of the DNA fishhook for detecting the Met dimer and miRNA-21; calculated VIE of different compounds; comparison of recent detection methods; recovery experiment; and oligonucleotide sequence (PDF)

## AUTHOR INFORMATION

### Corresponding Authors

**Xiaobing Huang** – Department of Medical Oncology, Fuzhou First Hospital Affiliated with Fujian Medical University, Fuzhou, Fujian Province 350009, PR China; Email: [13609522917@139.com](mailto:13609522917@139.com)

**Xi Zhang** – Innovative Drug Research Institute, Fujian Key Laboratory of Drug Target Discovery and Structural and Functional Research, The School of Pharmacy, and Department of Clinical Pharmacy and Pharmacy Administration, The School of Pharmacy, Fujian Medical University, Fuzhou, Fujian Province 350122, PR China; [orcid.org/0000-0001-5777-2368](https://orcid.org/0000-0001-5777-2368); Email: [xz@fjmu.edu.cn](mailto:xz@fjmu.edu.cn)

**Jinghua Chen** – Department of Pharmaceutical Analysis, The School of Pharmacy, Innovative Drug Research Institute, and Fujian Key Laboratory of Drug Target Discovery and Structural and Functional Research, The School of Pharmacy, Fujian Medical University, Fuzhou, Fujian Province 350122, PR China; [orcid.org/0000-0001-8718-0232](https://orcid.org/0000-0001-8718-0232); Email: [cjh\\_huaxue@126.com](mailto:cjh_huaxue@126.com)

### Authors

**Guanyu Chen** – Department of Pharmaceutics, The School of Pharmacy, Fujian Medical University, Fuzhou, Fujian Province 350122, PR China; Innovative Drug Research Institute and Fujian Key Laboratory of Drug Target Discovery and Structural and Functional Research, The School of Pharmacy, Fujian Medical University, Fuzhou, Fujian Province 350122, PR China; [orcid.org/0000-0002-6537-4682](https://orcid.org/0000-0002-6537-4682)

**Lilan Xu** – Department of Pharmaceutics, The School of Pharmacy, Fujian Medical University, Fuzhou, Fujian Province 350122, PR China; Innovative Drug Research Institute and Fujian Key Laboratory of Drug Target Discovery and Structural and Functional Research, The School of Pharmacy, Fujian Medical University, Fuzhou, Fujian Province 350122, PR China

**Zhuhua Chen** – Department of Pharmaceutical Analysis, The School of Pharmacy, Innovative Drug Research Institute, and Fujian Key Laboratory of Drug Target Discovery and Structural and Functional Research, The School of Pharmacy, Fujian Medical University, Fuzhou, Fujian Province 350122, PR China

**Lifang Lin** – Department of Pharmaceutical Analysis, The School of Pharmacy, Innovative Drug Research Institute, and Fujian Key Laboratory of Drug Target Discovery and Structural and Functional Research, The School of Pharmacy, Fujian Medical University, Fuzhou, Fujian Province 350122, PR China

**Wenlu Wang** – Innovative Drug Research Institute and Fujian Key Laboratory of Drug Target Discovery and Structural and Functional Research, The School of Pharmacy, Fujian Medical University, Fuzhou, Fujian Province 350122, PR China

**Mingzhu Chen** – Department of Pharmaceutical Analysis, The School of Pharmacy, Innovative Drug Research Institute, and Fujian Key Laboratory of Drug Target Discovery and Structural and Functional Research, The School of Pharmacy, Fujian Medical University, Fuzhou, Fujian Province 350122, PR China

**Weiming Sun** – Innovative Drug Research Institute and Fujian Key Laboratory of Drug Target Discovery and

Structural and Functional Research, The School of Pharmacy, Fujian Medical University, Fuzhou, Fujian Province 350122, PR China; [orcid.org/0000-0002-9882-0511](https://orcid.org/0000-0002-9882-0511)

Complete contact information is available at:

<https://pubs.acs.org/10.1021/acssensors.4c03142>

### Author Contributions

<sup>†</sup>G.C. and L.X. contributed equally to this work.

### Notes

The authors declare no competing financial interest.

## ACKNOWLEDGMENTS

The authors gratefully acknowledge the financial support of the Key technological innovation and industrialization projects of Fujian Province (2024XQ013), Science and Technology Plan Project of Fujian Province (2024Y4004), Natural Science Foundation of Fujian Province (2022J01207), Scientific Research Development Fund Project of Fujian Medical University (2022QH2233), and Fuzhou Science and Technology Innovation and Entrepreneurship Talent Cultivation Program Project (2023-R010). They would like to thank Zhihong Huang, who is from the Public Technology Service Center (Fujian Medical University), for technical assistance.

## REFERENCES

- (1) Wishart, D. S.; Bartok, B.; Oler, E.; Liang, K. Y. H.; Budinski, Z.; Berjanskii, M.; Guo, A.; Cao, X.; Wilson, M. MarkerDB: an online database of molecular biomarkers. *Nucleic Acids Res.* **2021**, *49*, D1259–D1267.
- (2) Chang, J.; Wang, X.; Wang, J.; Li, H.; Li, F. Nucleic Acid-Functionalized Metal–Organic Framework-Based Homogeneous Electrochemical Biosensor for Simultaneous Detection of Multiple Tumor Biomarkers. *Anal. Chem.* **2019**, *91*, 3604–3610.
- (3) Liu, X.; Wang, Q.; Li, J.; Diao, Z.; Hou, J.; Huo, D.; Hou, C. Simultaneous Detection of Micro-RNAs by a Disposable Biosensor via the Click Chemistry Connection Strategy. *Anal. Chem.* **2024**, *96*, 10577–10585.
- (4) Pakchin, P. S.; Nakhjavani, S. A.; Saber, R.; Ghanbari, H.; Omid, Y. Recent advances in simultaneous electrochemical multi-analyte sensing platforms. *TrAC, Trends Anal. Chem.* **2017**, *92*, 32–41.
- (5) Zhang, K.; Gao, H.; Deng, R.; Li, J. Emerging Applications of Nanotechnology for Controlling Cell-Surface Receptor Clustering. *Angew. Chem., Int. Ed.* **2019**, *58*, 4790–4799.
- (6) Li, D.; Liu, Y.; Li, Y.; Xiang, Y.; Yuan, R. Simultaneous and Sensitive Sensing of Intracellular MicroRNA and mRNA for the Detection of the PI3K/AKT Signaling Pathway in Live Cells. *Anal. Chem.* **2024**, *96*, 3329–3334.
- (7) Ma, X.; Chen, X.; Tang, Y.; Yan, R.; Miao, P. Triple-Input Molecular AND Logic Gates for Sensitive Detection of Multiple miRNAs. *ACS Appl. Mater. Interfaces* **2019**, *11*, 41157–41164.
- (8) Zhou, Z.; Sohn, Y. S.; Nechushtai, R.; Willner, I. DNA Tetrahedra Modules as Versatile Optical Sensing Platforms for multiplexed Analysis of miRNAs, Endonucleases, and Aptamer–Ligand Complexes. *ACS Nano* **2020**, *14*, 9021–9031.
- (9) Xu, S.; Chang, Y.; Wu, Z.; Li, Y.; Yuan, R.; Chai, Y. One DNA circle capture probe with multiple target recognition domains for simultaneous electrochemical detection of miRNA-21 and miRNA-155. *Biosens. Bioelectron.* **2020**, *149*, 111848.
- (10) Deng, Y.; Zhou, T.; Peng, Y.; Wang, M.; Xiang, L.; Zhang, Y.; Li, J.; Yang, J.; Li, G. Dual-Gene-Controlled Rolling Circle Amplification Strategy for SARS-CoV-2 Analysis. *Anal. Chem.* **2023**, *95*, 3358–3362.
- (11) Xu, E.; Feng, Y.; Yang, H.; Li, P.; Kong, L.; Wei, W.; Liu, S. Ultrasensitive and specific multi-miRNA detection based on dual signal amplification. *Sens. Actuators, B* **2021**, *337*, 129745.
- (12) Chikkaveeraiah, B. V.; Bhirde, A. A.; Morgan, N. Y.; Eden, H. S.; Chen, X. Electrochemical Immunosensors for Detection of Cancer Protein Biomarkers. *ACS Nano* **2012**, *6*, 6546–6561.
- (13) Fu, P.; King, S.; Xu, M.; Zhao, Y.; Zhao, C. Peptide nucleic acid-based electrochemical biosensor for simultaneous detection of multiple microRNAs from cancer cells with catalytic hairpin assembly amplification. *Sens. Actuators, B* **2020**, *305*, 127545.
- (14) Nano, A.; Furst, A. L.; Hill, M. G.; Barton, J. K. DNA Electrochemistry: Charge-Transport Pathways through DNA Films on Gold. *J. Am. Chem. Soc.* **2021**, *143*, 11631–11640.
- (15) Pei, H.; Zuo, X.; Pan, D.; Shi, J.; Huang, Q.; Fan, C. Scaffolded biosensors with designed DNA nanostructures. *NPG Asia Mater.* **2013**, *5*, No. e51.
- (16) Yuan, Y.-H.; Wu, Y.-D.; Chi, B.-Z.; Wen, S.-H.; Liang, R.-P.; Qiu, J.-D. Simultaneously electrochemical detection of microRNAs based on multifunctional magnetic nanoparticles probe coupling with hybridization chain reaction. *Biosens. Bioelectron.* **2017**, *97*, 325–331.
- (17) Jie, G.; Zhao, Y.; Wang, X.; Ding, C. multiplexed fluorescence detection of microRNAs based on novel distinguishable quantum dot signal probes by cycle amplification strategy. *Sens. Actuators, B* **2017**, *252*, 1026–1034.
- (18) Sánchez-Salcedo, R.; Miranda-Castro, R.; de-los-Santos-Álvarez, N.; Lobo-Castañón, M. J. Dual electrochemical genosensor for early diagnosis of prostate cancer through lncRNAs detection. *Biosens. Bioelectron.* **2021**, *192*, 113520.
- (19) Chaibun, T.; Puenpa, J.; Ngamdee, T.; Boonapatcharoen, N.; Athamanolap, P.; O'Mullane, A. P.; Vongpunsawad, S.; Poovorawan, Y.; Lee, S. Y.; Lertanantawong, B. Rapid electrochemical detection of coronavirus SARS-CoV-2. *Nat. Commun.* **2021**, *12*, 802.
- (20) Chang, Y.; Wu, Z.; Sun, Q.; Zhuo, Y.; Chai, Y.; Yuan, R. Simply Constructed and Highly Efficient Classified Cargo-Discharge DNA Robot: A DNA Walking Nanomachine Platform for Ultrasensitive multiplexed Sensing. *Anal. Chem.* **2019**, *91*, 8123–8128.
- (21) Sarwar, S.; Lin, M. C.; Ameza, C.; Wei, Z.; Iyayi, E.; Polk, H.; Wang, R.; Wang, H.; Zhang, X. Ultrasensitive electrochemical biosensors based on zinc sulfide/graphene hybrid for rapid detection of SARS-CoV-2. *Adv. Compos. Hybrid Mater.* **2023**, *6*, 49.
- (22) Roychoudhury, A.; Allen, R. J.; Curk, T.; Farrell, J.; McAllister, G.; Templeton, K.; Bachmann, T. T. Amplification Free Detection of SARS-CoV-2 Using Multi-Valent Binding. *ACS Sens.* **2022**, *7*, 3692–3699.
- (23) Yang, H.; Shen, H.; Qileng, A.; Cui, G.; Liang, Z.; Liu, Y.; Liu, W. Well-Aligned Track-Accelerated Tripedal DNA Walker for Photoelectrochemical Recognition of Dual-miRNAs Based on Molecular Logic Gates. *Anal. Chem.* **2023**, *95*, 5764–5772.
- (24) Han, Y.; Quan, K.; Feng, A.; Ye, M.; Sun, Y.; Zhang, K.; Xu, J.-J. Cyclic Enzymatic Signal Amplification-Driven DNA Logic Nano-devices on Framework Nucleic Acid for Highly Sensitive Electrochemiluminescence Detection of Dual Myocardial miRNAs. *Anal. Chem.* **2024**, *96*, 15728–15734.
- (25) Pei, H.; Lu, N.; Wen, Y.; Song, S.; Liu, Y.; Yan, H.; Fan, C. A DNA Nanostructure-based Biomolecular Probe Carrier Platform for Electrochemical Biosensing. *Adv. Mater.* **2010**, *22*, 4754–4758.
- (26) Zhong, Y.; Huang, L.-X.; Lin, M.-T.; Zhang, Z.-Y.; Liu, A.-L.; Lei, Y. A Y-shape-structured electrochemiluminescence biosensor based on carbon quantum dots and locked nucleic acid probe for microRNA determination with single-base resolution. *Biosens. Bioelectron.* **2023**, *238*, 115583.
- (27) Chen, G.; Chen, W.; Xu, L.; Jin, H.; Sun, W.; Lan, J.; Wu, F.; Zhang, X.; Zhang, J.; Chen, J. Sensitive, Highly Stable, and Anti-Fouling Electrode with Hexanethiol and Poly-A Modification for Exosomal microRNA Detection. *Anal. Chem.* **2022**, *94*, 5382–5391.
- (28) Zadeh, J. N.; Steenberg, C. D.; Bois, J. S.; Wolfe, B. R.; Pierce, M. B.; Khan, A. R.; Dirks, R. M.; Pierce, N. A. NUPACK: Analysis and design of nucleic acid systems. *J. Comput. Chem.* **2011**, *32*, 170–173.
- (29) Uzawa, T.; Cheng, R. R.; White, R. J.; Makarov, D. E.; Plaxco, K. W. A mechanistic study of electron transfer from the distal termini

of electrode-bound, single-stranded DNAs. *J. Am. Chem. Soc.* **2010**, *132*, 16120–16126.

(30) Furst, A. L.; Muren, N. B.; Hill, M. G.; Barton, J. K. Label-free electrochemical detection of human methyltransferase from tumors. *Proc. Natl. Acad. Sci. U.S.A.* **2014**, *111*, 14985–14989.

(31) Boon, E. M.; Ceres, D. M.; Drummond, T. G.; Hill, M. G.; Barton, J. K. Mutation detection by electrocatalysis at DNA-modified electrodes. *Nat. Biotechnol.* **2000**, *18*, 1096–1100.

(32) Tamura, S.-i.; Kokuchi, K.; Kokubun, H.; Weller, A. J. Z. f. P. C. Electron Transfer Reactions between Triplet Methylene Blue and Ferrocenes in Acetonitrile. *Z. Phys. Chem.* **1980**, *121*, 165–172.

(33) Ye, Y.-L.; Wang, W.-L.; Sun, W.-M.; Yang, J. Polymeric tungsten carbide nanoclusters as potential non-noble metal catalysts for CO oxidation. *Nanoscale* **2022**, *14*, 18231–18240.

(34) Ye, Y. L.; Pan, K. Y.; Wang, W. L.; Ni, B. L.; Sun, W. M. On the Catalytic Performance of  $(ZrO)_n$  ( $n=1-4$ ) Clusters for CO Oxidation: A DFT Study. *ChemPhysChem* **2023**, *24*, No. e202200776.

(35) Zhao, L.; Li, C.; Kang, X.; Li, Y. A visual detection strategy for SARS-CoV-2 based on dual targets-triggering DNA walker. *Sens. Actuators, B* **2023**, *379*, 133252.

(36) Zhang, Y.; Huang, X.; Li, W.; Xie, Q.; Zhang, J.; Luo, F.; Qiu, B.; Chen, Z.; Lin, Z.; Xu, G. Dual-target nucleic acid sequences responsive electrochemiluminescence biosensor using single type carbon dots as probe for SARS-CoV-2 detection based on series catalytic hairpin assembly amplification. *Sens. Actuators, B* **2023**, *379*, 133223.

(37) Rodríguez Díaz, C.; Lafuente-Gómez, N.; Coutinho, C.; Pardo, D.; Alarcón-Iniesta, H.; López-Valls, M.; Coloma, R.; Milán-Rois, P.; Domenech, M.; Abreu, M.; Cantón, R.; Galán, J. C.; Bocanegra, R.; Campos, L. A.; Miranda, R.; Castellanos, M.; Somoza, A. Development of colorimetric sensors based on gold nanoparticles for SARS-CoV-2 RdRp, E and S genes detection. *Talanta* **2022**, *243*, 123393.

(38) Azzouzi, S.; Fredj, Z.; Turner, A. P. F.; Ali, M. B.; Mak, W. C. Generic Neutravidin Biosensor for Simultaneous multiple Detection of MicroRNAs via Electrochemically Encoded Responsive Nanolabels. *ACS Sens.* **2019**, *4*, 326–334.

(39) Mamedov, M. R.; Vedova, S.; Freimer, J. W.; Sahu, A. D.; Ramesh, A.; Arce, M. M.; Meringa, A. D.; Ota, M.; Chen, P. A.; Hanspers, K.; Nguyen, V. Q.; Takeshima, K. A.; Rios, A. C.; Pritchard, J. K.; Kuball, J.; Sebestyen, Z.; Adams, E. J.; Marson, A. CRISPR screens decode cancer cell pathways that trigger  $\gamma\delta$  T cell detection. *Nature* **2023**, *621*, 188–195.

(40) Conway, J. R. ; Warren, S. C.; Lee, Y.-K.; McCulloch, A. T.; Magenau, A.; Lee, V.; Metcalf, X. L.; Stoehr, J.; Haigh, K.; Abdulkhalek, L.; Guaman, C. S.; Reed, D. A.; Murphy, K. J.; Pereira, B. A.; Méléneć, P.; Chambers, C.; Latham, S. L.; Lenthall, H.; Deenick, E. K.; Ma, Y.; Phan, T.; Lim, E.; Joshua, A. M.; Walters, S.; Grey, S. T.; Shi, Y.-C.; Zhang, L.; Herzog, H.; Croucher, D. R.; Philp, A.; Scheele, C. L. G. J.; Herrmann, D.; Sansom, O. J.; Morton, J. P.; Papa, A.; Haigh, J. J.; Nobis, M.; Timpson, P. Monitoring AKT activity and targeting in live tissue and disease contexts using a real-time Akt-FRET biosensor mouse. *Sci. Adv.* **2023**, *9*, No. eadf9063.

(41) Boldin, M. P.; Baltimore, D. MicroRNAs, new effectors and regulators of NF- $\kappa$ B. *Immunol. Rev.* **2012**, *246*, 205–220.

(42) Iliopoulos, D.; Jaeger, S. A.; Hirsch, H. A.; Bulyk, M. L.; Struhl, K. STAT3 Activation of miR-21 and miR-181b-1 via PTEN and CYLD Are Part of the Epigenetic Switch Linking Inflammation to Cancer. *Mol. Cell* **2010**, *39*, 493–506.